PERGAMON

International Journal of Solids and Structures 39 (2002) 5991–6010

INTERNATIONAL JOURNAL OF SOLIDS and STRUCTURES

www.elsevier.com/locate/ijsolstr

Postbuckling analysis of axially loaded functionally graded cylindrical panels in thermal environments

Hui-Shen Shen

School of Civil Engineering and Mechanics, Shanghai Jiao Tong University, 1954 Hua Shan Road, Shanghai 200030, China

Received 5 November 2001; received in revised form 18 July 2002

Abstract

A postbuckling analysis is presented for a functionally graded cylindrical panel of finite length subjected to axial compression in thermal environments. Material properties are assumed to be temperature dependent, and graded in the thickness direction according to a simple power law distribution in terms of the volume fractions of the constituents. The governing equations of a functionally graded cylindrical panel are based on Reddy's higher order shear deformation shell theory with a von Kármán–Donnell-type of kinematic nonlinearity and including thermal effects. Two cases of the in-plane boundary conditions are considered. The nonlinear prebuckling deformations and initial geometric imperfections of the panel are both taken into account. A boundary layer theory of shell buckling, which includes the effects of nonlinear prebuckling deformations, large deflections in the postbuckling range, and initial geometric imperfections of the shell, is extended to the case of functionally graded cylindrical panels under axial compression. A singular perturbation technique is employed to determine the buckling loads and postbuckling equilibrium paths. The numerical illustrations concern the postbuckling behavior of axially loaded, perfect and imperfect, functional graded cylindrical panels with two constituent materials and under different sets of thermal environments. The influences played by temperature rise, volume fraction distributions, the character of in-plane boundary conditions, transverse shear deformation, panel geometric parameters, as well as initial geometric imperfections are studied.

Keywords: Postbuckling; Functionally graded materials; Cylindrical panel; Shear deformation shell theory; Boundary layer theory of shell buckling; Singular perturbation technique

1. Introduction

Functionally graded materials (FGMs) have received considerable attention in many engineering applications since they were first reported in 1984 in Japan (see Koizumi, 1993). FGMs are composite materials, microscopically inhomogeneous, in which the mechanical properties vary smoothly and continuously from one surface to the other. This is achieved by gradually varying the volume fraction of the constituent materials. FGMs were initially designed as thermal barrier materials for aerospace structural applications and fusion reactors. FGMs are now developed for general use as structural components in

E-mail address: hsshen@mail.sjtu.edu.cn (H.-S. Shen).

0020-7683/02/$ - see front matter
PII: S0020-7683(02)00479-1

extremely high temperature environments. Unlike fiber–matrix composites which have a mismatch of mechanical properties across an interface of two discrete materials bonded together and may result in debonding at high temperatures, FGMs have the advantage of being able to withstand high temperature environments while maintaining their structural integrity. With the increased usage of these materials, it is important to understand the buckling and postbuckling behaviors of functionally graded cylindrical panels.

Many postbuckling studies, based on classical shell theory, of composite laminated thin cylindrical panels subjected to mechanical or thermal loading are available in the literature (see, for example Zhang and Matthews, 1985; Huang and Taucher, 1991). Relatively few studies involving the application of shear deformation shell theory to postbuckling analysis can be found in Chia (1987); Kweon and Hong (1994); Kweon et al. (1995); Chang and Librescu (1995), and Librescu et al. (2000). In these studies the material properties are considered to be independent of temperature. However, investigations of FGM cylindrical shells under mechanical or thermal loading are limited in number. Loy et al. (1999) gave a free vibration analysis of simply supported FGM cylindrical thin shells. This work is then extended to the case of FGM cylindrical thin shells under various boundary conditions by Pradhan et al. (2000). Ng et al. (2001) studied the parametric resonance or dynamic stability of FGM cylindrical thin shells under periodic axial loading. In the forgoing studies, Reddy and his co-workers developed a simple theory, in which the material properties are graded in the thickness direction according to a volume fraction power law distribution, but their numerical results were only for a simple case of an FGM shell in a fixed thermal environment. Recently, Shen (2002b) gave a postbuckling analysis of FGM cylindrical thin shells subjected to axial compression in thermal environments. Note that in the above studies the shells are considered as being relatively thin and therefore the transverse shear deformation is usually not accounted for.

It has been shown in Shen and Chen (1988, 1990) that in shell buckling, there is a boundary layer phenomenon where prebuckling and buckling displacement vary rapidly. They suggested a boundary layer theory of shell buckling, which includes the effects of nonlinear prebuckling deformations, large deflections in the postbuckling range, and initial geometric imperfections of the shell. Based on this theory, the postbuckling analyses for perfect and imperfect, unstiffened and stiffened, thin and moderately thick, isotropic and multilayered cylindrical shells under various loading cases have been performed by Shen and Chen (1990) and Shen (1997a,b,c, 1998, 2001a,b, 2002a,b). The present paper extends the previous works to the case of FGM cylindrical panels of finite length with two constituent materials subjected to compressive axial loads in thermal environments. The material properties are assumed to be temperature dependent, and graded in thickness direction according to a volume fraction power law distribution. The governing equations are based on Reddy's higher order shear deformation shell theory with a von Kármán–Donnell-type of kinematic nonlinearity and including thermal effects. A singular perturbation technique is employed to determine the buckling loads and postbuckling equilibrium paths. The nonlinear prebuckling deformations and initial geometric imperfections of the panel are both taken into account but, for simplicity, the form of initial geometric imperfection is assumed to be the same as the initial buckling mode of the panel. The numerical illustrations show the full nonlinear postbuckling response of FGM cylindrical panels subjected to axial compression and under different sets of environmental conditions.

2. Theoretical development

Consider an FGM cylindrical panel made from a mixture of ceramics and metals is subjected to axial compressive load P_0 combined with thermal loads. The panel is referred to a coordinate system (X, Y, Z) in which X and Y are in the axial and circumferential directions of the panel and Z is in the direction of the inward normal to the middle surface, the corresponding displacement designated by $\overline{U}$, $\overline{V}$ and $\overline{W}$. $\overline{\Psi}_x$ and $\overline{\Psi}_y$ are the rotations of normals to the middle surface with respect to the Y- and X-axes, respectively. The origin of the coordinate system is located at the corner of the panel on the middle plane. R is the radius of

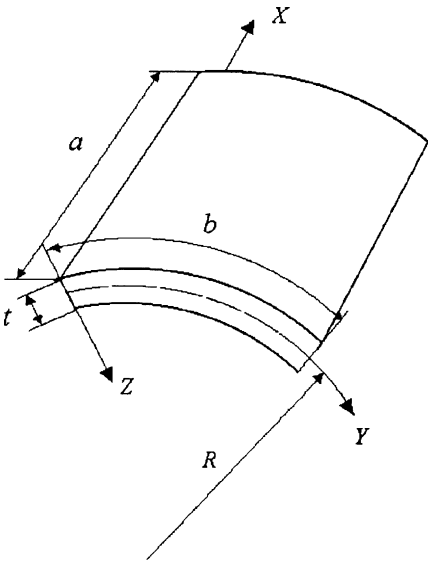

Fig. 1. Geometry and coordinate system of an FGM cylindrical panel.

curvature, t the panel thickness, a the length in the X-direction, and b the length in the Y-direction, as shown in Fig. 1. The panel is assumed to be geometrically imperfect. Denoting the initial geometric imperfection by $\overline{W}^*(X,Y)$, let $\overline{W}(X,Y)$ be the additional deflection and $\overline{F}(X,Y)$ be the stress function for the stress resultants defined by $\overline{N}_x = \overline{F}_{,yy}$, $\overline{N}_y = \overline{F}_{,xx}$ and $\overline{N}_{xy} = -\overline{F}_{,xy}$, where a comma denotes partial differentiation with respect to the corresponding coordinates.

We assume that the composition is varied from the outer to the inner surface, i.e. the outer surface ($Z = -t/2$) of the panel is ceramic-rich whereas the inner surface ($Z = t/2$) is metal-rich. In such a way, the effective material properties P, like Young's modulus E or thermal expansion coefficient α, can be expressed as

$$P = P_t V_c + P_b V_m \tag{1}$$

in which P_t and P_b denote the temperature-dependent properties of the outer and inner surfaces of the panel, respectively, and V_c and V_m are the ceramic and metal volume fractions and are related by

$$V_c + V_m = 1 \tag{2}$$

We assume the volume fraction V_m follows a simple power law as

$$V_m = \left(\frac{2Z+t}{2t}\right)^N \tag{3}$$

where volume fraction index N dictates the material variation profile through the panel thickness and may be varied to obtain the optimum distribution of component materials. It is noted that similar definition can be found in Ng et al. (2001), but is for V_c.

From Eqs. (1)–(3), the effective Young's modulus E and thermal expansion coefficient α of an FGM cylindrical panel can be written as

$$E = (E_b - E_t)\left(\frac{2Z+t}{2t}\right)^N + E_t, \qquad \alpha = (\alpha_b - \alpha_t)\left(\frac{2Z+t}{2t}\right)^N + \alpha_t \tag{4}$$

It is evident that when $Z = -t/2$, $E = E_t$ and $\alpha = \alpha_t$, and when $Z = t/2$, $E = E_b$ and $\alpha = \alpha_b$. It is assumed that E_t, E_b, α_t and α_b are functions of temperature, but Poisson's ratio v depends weakly on temperature

change and is assumed to be a constant, as shown in Section 4, so that E and α are functions of temperature and position.

Reddy and Liu (1985) developed a simple higher order shear deformation shell theory, in which the transverse shear strains are assumed to be parabolically distributed across the shell thickness and which contains the same dependent unknowns as in the first order shear deformation theory. Based on Reddy's higher order shear deformation theory with von Kármán–Donnell-type kinematic relations and including thermal effects, the governing differential equations for an FGM cylindrical panel are derived and can be expressed in terms of a stress function $\overline{F}$, two rotations $\overline{\Psi}_x$ and $\overline{\Psi}_y$, and transverse displacement $\overline{W}$, along with initial geometric imperfection $\overline{W}^*$. They are

$$\widetilde{L}_{11}(\overline{W}) - \widetilde{L}_{12}(\overline{\Psi}_x) - \widetilde{L}_{13}(\overline{\Psi}_y) + \widetilde{L}_{14}(\overline{F}) - \widetilde{L}_{15}(\overline{N}^{\mathrm{T}}) - \widetilde{L}_{16}(\overline{M}^{\mathrm{T}}) - \frac{1}{R}\overline{F}_{,xx} = \widetilde{L}(\overline{W} + \overline{W}^*, \overline{F}) \tag{5}$$

$$\widetilde{L}_{21}(\overline{F}) + \widetilde{L}_{22}(\overline{\Psi}_x) + \widetilde{L}_{23}(\overline{\Psi}_y) - \widetilde{L}_{24}(\overline{W}) - \widetilde{L}_{25}(\overline{N}^{\mathrm{T}}) + \frac{1}{R}\overline{W}_{,xx} = -\frac{1}{2}\widetilde{L}(\overline{W} + 2\overline{W}^*, \overline{W}) \tag{6}$$

$$\widetilde{L}_{31}(\overline{W}) + \widetilde{L}_{32}(\overline{\Psi}_x) - \widetilde{L}_{33}(\overline{\Psi}_y) + \widetilde{L}_{34}(\overline{F}) - \widetilde{L}_{35}(\overline{N}^{\mathrm{T}}) - \widetilde{L}_{36}(\overline{S}^{\mathrm{T}}) = 0 \tag{7}$$

$$\widetilde{L}_{41}(\overline{W}) - \widetilde{L}_{42}(\overline{\Psi}_x) + \widetilde{L}_{43}(\overline{\Psi}_y) + \widetilde{L}_{44}(\overline{F}) - \widetilde{L}_{45}(\overline{N}^{\mathrm{T}}) - \widetilde{L}_{46}(\overline{S}^{\mathrm{T}}) = 0 \tag{8}$$

where linear operators $\widetilde{L}_{ij}(\ )$ and nonlinear operator $\widetilde{L}(\ )$ are defined as in Shen (2002c).

It is noted that these panel equations show thermal coupling as well as the interaction of stretching and bending. Also, note that Eqs. (5)–(8) are identical to those of unsymmetric cross-ply laminated cylindrical shells under thermomechanical loading.

The forces, moments and higher order moments caused by elevated temperature are defined by

$$\begin{bmatrix} \overline{N}_x^{\mathrm{T}} & \overline{M}_x^{\mathrm{T}} & \overline{P}_x^{\mathrm{T}} \\ \overline{N}_y^{\mathrm{T}} & \overline{M}_y^{\mathrm{T}} & \overline{P}_y^{\mathrm{T}} \\ \overline{N}_{xy}^{\mathrm{T}} & \overline{M}_{xy}^{\mathrm{T}} & \overline{P}_{xy}^{\mathrm{T}} \end{bmatrix} = \int_{-t/2}^{t/2} (1, Z, Z^3) \begin{bmatrix} A_x \\ A_y \\ A_{xy} \end{bmatrix} \Delta T \, \mathrm{d}Z \tag{9a}$$

$$\begin{bmatrix} \overline{S}_x^{\mathrm{T}} \\ \overline{S}_y^{\mathrm{T}} \\ \overline{S}_{xy}^{\mathrm{T}} \end{bmatrix} = \begin{bmatrix} \overline{M}_x^{\mathrm{T}} \\ \overline{M}_y^{\mathrm{T}} \\ \overline{M}_{xy}^{\mathrm{T}} \end{bmatrix} - \frac{4}{3t^2} \begin{bmatrix} \overline{P}_x^{\mathrm{T}} \\ \overline{P}_y^{\mathrm{T}} \\ \overline{P}_{xy}^{\mathrm{T}} \end{bmatrix} \tag{9b}$$

where ΔT is temperature rise from some reference temperature at which there are no thermal strains, and

$$\begin{bmatrix} A_x \\ A_y \\ A_{xy} \end{bmatrix} = -\begin{bmatrix} Q_{11} & Q_{12} & Q_{16} \\ Q_{12} & Q_{22} & Q_{26} \\ Q_{16} & Q_{26} & Q_{66} \end{bmatrix} \begin{bmatrix} 1 & 0 \\ 0 & 1 \\ 0 & 0 \end{bmatrix} \begin{bmatrix} \alpha \\ \alpha \end{bmatrix} \tag{10}$$

where the thermal expansion coefficient α is given in detail in Eq. (4), and

$$Q_{11} = Q_{22} = \frac{E}{1-\nu^2}, \quad Q_{12} = \frac{\nu E}{1-\nu^2}, \quad Q_{16} = Q_{26} = 0, \quad Q_{44} = Q_{55} = Q_{66} = \frac{E}{2(1+\nu)} \tag{11}$$

in which E is also given in detail in Eq. (4),and vary through the panel thickness.

All four edges are assumed to be simply supported. Depending upon the in-plane behavior at the edges, two cases, Case 1 (referred to herein as movable edges) and Case 2 (referred to herein as immovable edges), will be considered.

Case 1: The edges are simply supported and freely movable in the X- and Y-directions, respectively.

Case 2: All four edges are simply supported. Uniaxial edge loads are acting in the X-direction. The curved edges ($X = 0, a$) are considered freely movable (in the in-plane direction), the remaining two straight edges being unloaded and immovable (in the Y-direction).

For both cases the associated boundary conditions could be found in Chang and Librescu (1995). In the present paper, they are

$X = 0, a$:

$$\overline{W} = \overline{V} = \overline{\Psi}_y = 0 \tag{12a}$$

$$\overline{M}_x = \overline{P}_x = 0 \tag{12b}$$

$$\int_0^b \overline{N}_x \,\mathrm{d}Y + \sigma_x t b = 0 \tag{12c}$$

$Y = 0, b$:

$$\overline{W} = \overline{\Psi}_x = 0 \tag{12d}$$

$$\overline{N}_{xy} = 0 \tag{12e}$$

$$\int_0^a \overline{N}_y \,\mathrm{d}X = 0 \quad \text{(movable edges)} \tag{12f}$$

$$\overline{V} = 0 \quad \text{(immovable edges)} \tag{12g}$$

where σ_x is the average axial compressive stress, $\overline{M}_x$ is the bending moment and $\overline{P}_x$ is higher order moment as defined in Reddy and Liu (1985). The condition expressing the immovability condition $\overline{V} = 0$ (on $Y = 0, b$) is fulfilled on the average sense as (Chang and Librescu, 1995)

$$\int_0^a \int_0^b \frac{\partial \overline{V}}{\partial Y} \mathrm{d}Y \,\mathrm{d}X = 0 \tag{13a}$$

or

$$\int_0^a \int_0^b \left[A_{22}^* \frac{\partial^2 \overline{F}}{\partial X^2} + A_{12}^* \frac{\partial^2 \overline{F}}{\partial Y^2} + \left(B_{21}^* - \frac{4}{3t^2} E_{21}^* \right) \frac{\partial \overline{\Psi}_x}{\partial X} + \left(B_{22}^* - \frac{4}{3t^2} E_{22}^* \right) \frac{\partial \overline{\Psi}_y}{\partial Y} - \frac{4}{3t^2} \left(E_{21}^* \frac{\partial^2 \overline{W}}{\partial X^2} + E_{22}^* \frac{\partial^2 \overline{W}}{\partial Y^2} \right) + \frac{\overline{W}}{R} - \frac{1}{2} \left(\frac{\partial \overline{W}}{\partial Y} \right)^2 - \frac{\partial \overline{W}}{\partial Y} \frac{\partial \overline{W}^*}{\partial Y} - \left(A_{12}^* \overline{N}_x^{\mathrm{T}} + A_{22}^* \overline{N}_y^{\mathrm{T}} \right) \right] \mathrm{d}Y \,\mathrm{d}X = 0 \tag{13b}$$

The average end-shortening relationship is

$$\begin{aligned} \frac{\Delta_x}{a} &= -\frac{1}{ab} \int_0^b \int_0^a \frac{\partial \overline{U}}{\partial X} \mathrm{d}X \,\mathrm{d}Y \\ &= -\frac{1}{ab} \int_0^b \int_0^a \left[A_{11}^* \frac{\partial^2 \overline{F}}{\partial Y^2} + A_{12}^* \frac{\partial^2 \overline{F}}{\partial X^2} + \left(B_{11}^* - \frac{4}{3t^2} E_{11}^* \right) \frac{\partial \overline{\Psi}_x}{\partial X} + \left(B_{12}^* - \frac{4}{3t^2} E_{12}^* \right) \frac{\partial \overline{\Psi}_y}{\partial Y} \right. \\ &\quad \left. - \frac{4}{3t^2} \left(E_{11}^* \frac{\partial^2 \overline{W}}{\partial X^2} + E_{12}^* \frac{\partial^2 \overline{W}}{\partial Y^2} \right) - \frac{1}{2} \left(\frac{\partial \overline{W}}{\partial X} \right)^2 - \frac{\partial \overline{W}}{\partial X} \frac{\partial \overline{W}^*}{\partial X} - \left(A_{11}^* \overline{N}_x^{\mathrm{T}} + A_{12}^* \overline{N}_y^{\mathrm{T}} \right) \right] \mathrm{d}X \,\mathrm{d}Y \end{aligned} \tag{14}$$

In Eqs. (13b), (14) and Eq. (17) below, the reduced stiffness matrices $[A^*_{ij}]$, $[B^*_{ij}]$, $[D^*_{ij}]$, $[E^*_{ij}]$, $[F^*_{iJ}]$ and $[H^*_{ij}]$ $(i,j=1,2,6)$ are functions of temperature and position, defined by

$$\mathbf{A}^* = \mathbf{A}^{-1}, \quad \mathbf{B}^* = -\mathbf{A}^{-1}\mathbf{B}, \quad \mathbf{D}^* = \mathbf{D} - \mathbf{B}\mathbf{A}^{-1}\mathbf{B}, \quad \mathbf{E}^* = -\mathbf{A}^{-1}\mathbf{E}, \quad \mathbf{F}^* = \mathbf{F} - \mathbf{E}\mathbf{A}^{-1}\mathbf{B},$$
$$\mathbf{H}^* = \mathbf{H} - \mathbf{E}\mathbf{A}^{-1}\mathbf{E} \tag{15}$$

where A_{ij}, B_{ij} etc., are the panel stiffnesses, defined by

$$(A_{ij}, B_{ij}, D_{ij}, E_{ij}, F_{ij}, H_{ij}) = \int_{-t/2}^{t/2} (Q_{ij})(1, Z, Z^2, Z^3, Z^4, Z^6)\,\mathrm{d}Z, \quad i,j = 1,2,6 \tag{16a}$$

$$(A_{ij}, D_{ij}, F_{ij}) = \int_{-t/2}^{t/2} (Q_{ij})(1, Z^2, Z^4)\,\mathrm{d}Z, \quad i,j = 4,5 \tag{16b}$$

3. Analytical method and asymptotic solutions

Having developed the theory, we now try to solve Eqs. (5)–(8) with boundary conditions (12a)–(12g). Before proceeding, it is convenient first to define the following dimensionless quantities (with γ_{ijk} in Eqs. (23), (25) and (26) below are defined as in Shen (2002c))

$$\begin{aligned}
&x = \pi X/a, \quad y = \pi Y/b, \quad \beta = a/b, \quad \overline{Z} = a^2/Rt, \quad \varepsilon = (\pi^2 R/a^2)[D^*_{11}D^*_{22}A^*_{11}A^*_{22}]^{1/4},\\
&(W, W^*) = \varepsilon(\overline{W}, \overline{W}^*)/[D^*_{11}D^*_{22}A^*_{11}A^*_{22}]^{1/4}, \quad F = \varepsilon^2\overline{F}/[D^*_{11}D^*_{22}]^{1/2},\\
&(\Psi_x, \Psi_y) = \varepsilon^2(\overline{\Psi}_x, \overline{\Psi}_y)(a/\pi)/[D^*_{11}D^*_{22}A^*_{11}A^*_{22}]^{1/4},\\
&\gamma_{14} = [D^*_{22}/D^*_{11}]^{1/2}, \quad \gamma_{24} = [A^*_{11}/A^*_{22}]^{1/2}, \quad \gamma_5 = -A^*_{12}/A^*_{22},\\
&(\gamma_{31}, \gamma_{41}) = (a^2/\pi^2)(A_{55} - 8D_{55}/t^2 + 16F_{55}/t^4, A_{44} - 8D_{44}/t^2 + 16F_{44}/t^4)/D^*_{11}\\
&(\gamma_{T1}, \gamma_{T2}) = (A^T_x, A^T_y)R[A^*_{11}A^*_{22}/D^*_{11}D^*_{22}]^{1/4},\\
&(M_x, P_x, M^T_x, P^T_x) = \varepsilon^2(\overline{M}_x, 4\overline{P}_x/3t^2, \overline{M}^T_x, 4\overline{P}^T_x/3t^2)a^2/\pi^2 D^*_{11}[D^*_{11}D^*_{12}A^*_{11}A^*_{12}]^{1/4},\\
&\lambda_p = \sigma_x/(2/Rt)[D^*_{11}D^*_{22}/A^*_{11}A^*_{22}]^{1/4}, \quad \delta_p = (\Delta_x/a)/(2/R)[D^*_{11}D^*_{22}A^*_{11}A^*_{22}]^{1/4}
\end{aligned} \tag{17}$$

in which $A^T_x = A^T_y$ are defined by

$$\begin{bmatrix} A^T_x \\ A^T_y \end{bmatrix} = -\int_{-t/2}^{t/2} \begin{bmatrix} A_x \\ A_y \end{bmatrix} \mathrm{d}Z \tag{18}$$

and the details of which can be found in Appendix A.

The nonlinear equations (5)–(8) may then be written in dimensionless form as

$$\varepsilon^2 L_{11}(W) - \varepsilon L_{12}(\Psi_x) - \varepsilon L_{13}(\Psi_y) + \varepsilon\gamma_{14}L_{14}(F) - \gamma_{14}F_{,xx} = \gamma_{14}\beta^2 L(W + W^*_T, F) \tag{19}$$

$$L_{21}(F) + \gamma_{24}L_{22}(\Psi_x) + \gamma_{24}L_{23}(\Psi_y) - \varepsilon\gamma_{24}L_{24}(W) + \gamma_{24}W_{,xx} = -\frac{1}{2}\gamma_{24}\beta^2 L(W + 2W^*_T, W) \tag{20}$$

$$\varepsilon L_{31}(W) + L_{32}(\Psi_x) - L_{33}(\Psi_y) + \gamma_{14}L_{34}(F) = 0 \tag{21}$$

$$\varepsilon L_{41}(W) - L_{42}(\Psi_x) + L_{43}(\Psi_y) + \gamma_{14}L_{44}(F) = 0 \tag{22}$$

where $W_{\mathrm{T}}^{*} = W^{*} + W_{\mathrm{II}}^{*}$, and W_{II}^{*} is the additional deflection caused by additional compressive stresses that develop in the panel with immovable edges, and for the case of movable straight edges $W_{\mathrm{II}}^{*} = 0$. In Eqs. (19)–(22) the operators become

$$L_{11}(\ ) = \gamma_{110}\frac{\partial^4}{\partial x^4} + 2\gamma_{112}\beta^2\frac{\partial^4}{\partial x^2\,\partial y^2} + \gamma_{114}\beta^4\frac{\partial^4}{\partial y^4}$$

$$L_{12}(\ ) = \gamma_{120}\frac{\partial^3}{\partial x^3} + \gamma_{122}\beta^2\frac{\partial^3}{\partial x\,\partial y^2}$$

$$L_{13}(\ ) = \gamma_{131}\beta\frac{\partial^3}{\partial x^2\,\partial y} + \gamma_{133}\beta^3\frac{\partial^3}{\partial y^3}$$

$$L_{14}(\ ) = \gamma_{140}\frac{\partial^4}{\partial x^4} + 2\gamma_{142}\beta^2\frac{\partial^4}{\partial x^2\,\partial y^2} + \gamma_{144}\beta^4\frac{\partial^4}{\partial y^4}$$

$$L_{21}(\ ) = \frac{\partial^4}{\partial x^4} + 2\gamma_{212}\beta^2\frac{\partial^4}{\partial x^2\,\partial y^2} + \gamma_{214}\beta^4\frac{\partial^4}{\partial y^4}$$

$$L_{22}(\ ) = \gamma_{220}\frac{\partial^3}{\partial x^3} + \gamma_{222}\beta^2\frac{\partial^3}{\partial x\,\partial y^2}$$

$$L_{23}(\ ) = \gamma_{231}\beta\frac{\partial^3}{\partial x^2\,\partial y} + \gamma_{233}\beta^3\frac{\partial^3}{\partial y^3}$$

$$L_{24}(\ ) = \gamma_{240}\frac{\partial^4}{\partial x^4} + 2\gamma_{242}\beta^2\frac{\partial^4}{\partial x^2\,\partial y^2} + \gamma_{244}\beta^4\frac{\partial^4}{\partial y^4}$$

$$L_{31}(\ ) = \gamma_{31}\frac{\partial}{\partial x} + \gamma_{310}\frac{\partial^3}{\partial x^3} + \gamma_{312}\beta^2\frac{\partial^3}{\partial x\,\partial y^2}$$

$$L_{32}(\ ) = \gamma_{31} - \gamma_{320}\frac{\partial^2}{\partial x^2} - \gamma_{322}\beta^2\frac{\partial^2}{\partial y^2}$$

$$L_{33}(\ ) = \gamma_{331}\beta\frac{\partial^2}{\partial x\,\partial y}$$

$$L_{34}(\ ) = L_{22}(\ )$$

$$L_{41}(\ ) = \gamma_{41}\beta\frac{\partial}{\partial y} + \gamma_{411}\beta\frac{\partial^3}{\partial x^2\,\partial y} + \gamma_{413}\beta^3\frac{\partial^3}{\partial y^3}$$

$$L_{42}(\ ) = L_{33}(\ )$$

$$L_{43}(\ ) = \gamma_{41} - \gamma_{430}\frac{\partial^2}{\partial x^2} - \gamma_{432}\beta^2\frac{\partial^2}{\partial y^2}$$

$$L_{44}(\ ) = L_{23}(\ )$$

$$L(\ ) = \frac{\partial^2}{\partial x^2}\frac{\partial^2}{\partial y^2} - 2\frac{\partial^2}{\partial x\,\partial y}\frac{\partial^2}{\partial x\,\partial y} + \frac{\partial^2}{\partial y^2}\frac{\partial^2}{\partial x^2} \tag{23}$$

Because of the definition of ε given in Eq. (17), for most of the FGMs $[D_{11}^{*}D_{22}^{*}A_{11}^{*}A_{22}^{*}]^{1/4} \cong 0.3t$, hence when $\overline{Z} = (a^2/Rt) > 2.96$, we have $\varepsilon < 1$. In particular, for homogeneous isotropic cylindrical panels, we have $\varepsilon = \pi^2/\overline{Z}_{\mathrm{V}}\beta^2[12(1-\nu^2)]^{1/2}$, where $\overline{Z}_{\mathrm{V}}(= b^2/Rt)$ should be greater than 11.95 in the case of classical linear buckling analysis (see Vol'mir, 1967), and in such a case $\varepsilon < 1$ is always valid unless $\beta < 0.5$. When $\varepsilon < 1$, Eqs. (19)–(22) are equations of the boundary layer type, from which nonlinear prebuckling deformations, large deflections in the postbuckling range and initial geometric imperfections of the panel can be considered simultaneously.

The boundary conditions of Eqs. (12a)–(12g) become

$x = 0, \pi$:

$$W = V = \Psi_y = 0 \tag{24a}$$

$$M_x = P_x = 0 \tag{24b}$$

$$\frac{1}{\pi}\int_0^{\pi} \beta^2 \frac{\partial^2 F}{\partial y^2}\,\mathrm{d}y + 2\lambda_{\mathrm{p}}\varepsilon = 0 \tag{24c}$$

$y = 0, \pi$:

$$W = \Psi_x = 0 \tag{24d}$$

$$F_{,xy} = 0 \tag{24e}$$

$$\int_0^{\pi} \frac{\partial^2 F}{\partial x^2}\,\mathrm{d}x = 0 \quad \text{(movable edges)} \tag{24f}$$

$$V = 0 \quad \text{(immovable edges)} \tag{24g}$$

The in-plane boundary condition expressed by Eq. (13b) becomes

$$\int_0^{\pi}\int_0^{\pi}\left[\left(\frac{\partial^2 F}{\partial x^2} - \gamma_5\beta^2\frac{\partial^2 F}{\partial y^2}\right) + \gamma_{24}\left(\gamma_{220}\frac{\partial \Psi_x}{\partial x} + \gamma_{522}\beta\frac{\partial \Psi_y}{\partial y}\right) - \varepsilon\gamma_{24}\left(\gamma_{240}\frac{\partial^2 W}{\partial x^2} + \gamma_{622}\beta^2\frac{\partial^2 W}{\partial y^2}\right) + \gamma_{24}W - \frac{1}{2}\gamma_{24}\beta^2\left(\frac{\partial W}{\partial y}\right)^2 - \gamma_{24}\beta^2\frac{\partial W}{\partial y}\frac{\partial W_{\mathrm{T}}^{*}}{\partial y} + \varepsilon(\gamma_{\mathrm{T2}} - \gamma_5\gamma_{\mathrm{T1}})\Delta T\right]\mathrm{d}y\,\mathrm{d}x = 0 \tag{25}$$

The unit end-shortening relationship becomes

$$\delta_{\mathrm{p}} = -\frac{1}{2\pi^2\gamma_{24}}\varepsilon^{-1}\int_0^{\pi}\int_0^{\pi}\left[\left(\gamma_{24}^2\beta^2\frac{\partial^2 F}{\partial y^2} - \gamma_5\frac{\partial^2 F}{\partial x^2}\right) + \gamma_{24}\left(\gamma_{511}\frac{\partial \Psi_x}{\partial x} + \gamma_{233}\beta\frac{\partial \Psi_y}{\partial y}\right) - \varepsilon\gamma_{24}\left(\gamma_{611}\frac{\partial^2 W}{\partial x^2} + \gamma_{244}\beta^2\frac{\partial^2 W}{\partial y^2}\right) - \frac{1}{2}\gamma_{24}\left(\frac{\partial W}{\partial x}\right)^2 - \gamma_{24}\frac{\partial W}{\partial x}\frac{\partial W_{\mathrm{T}}^{*}}{\partial x} + \varepsilon(\gamma_{24}^2\gamma_{\mathrm{T1}} - \gamma_5\gamma_{\mathrm{T2}})\Delta T\right]\mathrm{d}x\,\mathrm{d}y = 0 \tag{26}$$

By virtue of the fact that ΔT is assumed to be uniform, the thermal coupling in Eqs. (5)–(8) vanishes, but terms in ΔT intervene in Eqs. (25) and (26).

Applying Eqs. (19)–(23), (24a)–(24g), (25), (26), the postbuckling behavior of perfect and imperfect, FGM cylindrical panels subjected to axial compression and under thermal environments is determined by a singular perturbation technique. The essence of this procedure, in the present case, is to assume that

$$
\begin{aligned}
W &= w(x,y,\varepsilon) + \widetilde{W}(x,\xi,y,\varepsilon) + \widehat{W}(x,\varsigma,y,\varepsilon)\\
F &= f(x,y,\varepsilon) + \widetilde{F}(x,\xi,y,\varepsilon) + \widehat{F}(x,\varsigma,y,\varepsilon)\\
\Psi_x &= \psi_x(x,y,\varepsilon) + \widetilde{\Psi}_x(x,\xi,y,\varepsilon) + \widehat{\Psi}_x(x,\varsigma,y,\varepsilon)\\
\Psi_y &= \psi_y(x,y,\varepsilon) + \widetilde{\Psi}_y(x,\xi,y,\varepsilon) + \widehat{\Psi}_y(x,\varsigma,y,\varepsilon)
\end{aligned}
\tag{27}
$$

where ε is a small perturbation parameter (under the limitation of $\overline{Z} > 2.96$) and $w(x,y,\varepsilon)$, $f(x,y,\varepsilon)$, $\psi_x(x,y,\varepsilon)$, $\psi_y(x,y,\varepsilon)$ are called outer solutions or regular solutions of the panel, $\widetilde{W}(x,\xi,y,\varepsilon)$, $\widetilde{F}(x,\xi,y,\varepsilon)$, $\widetilde{\Psi}_x(x,\xi,y,\varepsilon)$, $\widetilde{\Psi}_y(x,\xi,y,\varepsilon)$ and $\widehat{W}(x,\varsigma,y,\varepsilon)$, $\widehat{F}(x,\varsigma,y,\varepsilon)$, $\widehat{\Psi}_x(x,\varsigma,y,\varepsilon)$, $\widehat{\Psi}_y(x,\varsigma,y,\varepsilon)$ are the boundary layer solutions near the $x = 0$ and $x = \pi$ edges, respectively, and ξ and ς are the boundary layer variables, defined as

$$
\xi = x/\sqrt{\varepsilon}, \quad \varsigma = (\pi - x)/\sqrt{\varepsilon} \tag{28}
$$

(This means for homogeneous isotropic cylindrical panels the width of the boundary layers is of order $\sqrt{Rt}$.) In Eq. (27) the regular and boundary layer solutions are taken in the form of perturbation expansions as

$$
\begin{aligned}
w(x,y,\varepsilon) &= \sum_{j=1} \varepsilon^j w_j(x,y), \quad f(x,y,\varepsilon) = \sum_{j=0} \varepsilon^j f_i(x,y)\\
\psi_x(x,y,\varepsilon) &= \sum_{j=1} \varepsilon^j (\psi_x)_j(x,y), \quad \psi_y(x,y,\varepsilon) = \sum_{j=1} \varepsilon^j (\psi_y)_j(x,y)
\end{aligned}
\tag{29a}
$$

$$
\begin{aligned}
\widetilde{W}(x,\xi,y,\varepsilon) &= \sum_{j=0} \varepsilon^{j+1} \widetilde{W}_{j+1}(x,\xi,y), \quad \widetilde{F}(x,\xi,y,\varepsilon) = \sum_{j=0} \varepsilon^{j+2} \widetilde{F}_{j+2}(x,\xi,y)\\
\widetilde{\Psi}_x(x,\xi,y,\varepsilon) &= \sum_{j=0} \varepsilon^{j+3/2} (\widetilde{\Psi}_x)_{j+3/2}(x,\xi,y), \quad \widetilde{\Psi}_y(x,\xi,y,\varepsilon) = \sum_{j=0} \varepsilon^{j+2} (\widetilde{\Psi}_y)_{j+2}(x,\xi,y)
\end{aligned}
\tag{29b}
$$

$$
\begin{aligned}
\widehat{W}(x,\varsigma,y,\varepsilon) &= \sum_{j=0} \varepsilon^{j+1} \widehat{W}_{j+1}(x,\varsigma,y), \quad \widehat{F}(x,\varsigma,y,\varepsilon) = \sum_{j=0} \varepsilon^{j+2} \widehat{F}_{j+2}(x,\varsigma,y)\\
\hat{\Psi}_x(x,\varsigma,y,\varepsilon) &= \sum_{j=0} \varepsilon^{j+3/2} (\widehat{\Psi}_x)_{j+3/2}(x,\varsigma,y), \quad \widehat{\Psi}_y(x,\varsigma,y,\varepsilon) = \sum_{j=0} \varepsilon^{j+2} (\widehat{\Psi}_y)_{j+2}(x,\varsigma,y)
\end{aligned}
\tag{29c}
$$

The initial buckling mode is assumed to have the form

$$
w_2(x,y) = A_{11}^{(2)} \sin mx \sin ny \tag{30}
$$

It should be remembered that, because of the definition of W given in Eq. (17), this means that $w_2(x,y)$ corresponds to $\bar{w}_1(X,Y)$ and the initial geometric imperfection is assumed to have the similar form

$$
W^*(x,y,\varepsilon) = \varepsilon^2 a_{11}^* \sin mx \sin ny \tag{31}
$$

Substituting Eqs. (27), (28), (29a)–(29c) into Eqs. (19)–(22), and collecting terms of the same order of ε, we obtain three sets of perturbation equations for the regular and boundary layer solutions, respectively.

Then using Eqs. (30) and (31) to solve these perturbation equations of each order, and matching the regular solutions with the boundary layer solutions at each end of the panel, so that the asymptotic solutions are constructed as

$$
\begin{aligned}
W = \varepsilon\Bigg[& A_{00}^{(1)} - A_{00}^{(1)}\left(a_{01}^{(1)}\cos\phi\frac{x}{\sqrt{\varepsilon}} + a_{10}^{(1)}\sin\phi\frac{x}{\sqrt{\varepsilon}}\right)\exp\left(-\alpha\frac{x}{\sqrt{\varepsilon}}\right) \\
& - A_{00}^{(1)}\left(a_{01}^{(1)}\cos\phi\frac{\pi-x}{\sqrt{\varepsilon}} + a_{10}^{(1)}\sin\phi\frac{\pi-x}{\sqrt{\varepsilon}}\right)\exp\left(-\alpha\frac{\pi-x}{\sqrt{\varepsilon}}\right)\Bigg] \\
& + \varepsilon^2\Bigg[A_{02}^{(2)}\sin mx\sin ny + A_{02}^{(2)}(\cos 2ny-1) - A_{02}^{(2)}(\cos 2ny-1)\left(a_{01}^{(1)}\cos\phi\frac{x}{\sqrt{\varepsilon}} + a_{10}^{(1)}\sin\phi\frac{x}{\sqrt{\varepsilon}}\right) \\
& \times\exp\left(-\alpha\frac{x}{\sqrt{\varepsilon}}\right) - A_{02}^{(2)}(\cos 2ny-1)\left(a_{01}^{(1)}\cos\phi\frac{\pi-x}{\sqrt{\varepsilon}} + a_{10}^{(1)}\sin\phi\frac{\pi-x}{\sqrt{\varepsilon}}\right) \\
& \times\exp\left(-\alpha\frac{\pi-x}{\sqrt{\varepsilon}}\right)\Bigg] + \varepsilon^3\left[A_{11}^{(3)}\sin mx\sin ny + A_{02}^{(3)}(\cos 2ny-1)\right] \\
& + \varepsilon^4\left[A_{00}^{(4)} + A_{20}^{(4)}\cos 2mx + A_{02}^{(4)}(\cos 2ny-1) + A_{13}^{(4)}\sin mx\sin 3ny + A_{04}^{(4)}(\cos 4ny-1)\right] + \mathrm{O}(\varepsilon^5)
\end{aligned}
\tag{32}
$$

$$
\begin{aligned}
F = & -B_{00}^{(0)}\frac{y^2}{2} + \varepsilon\left[-B_{00}^{(1)}\frac{y^2}{2}\right] + \varepsilon^2\Bigg[-B_{00}^{(2)}\frac{y^2}{2} + B_{11}^{(2)}\sin mx\sin ny + A_{00}^{(1)}\left(b_{01}^{(2)}\cos\phi\frac{x}{\sqrt{\varepsilon}} + b_{10}^{(2)}\sin\phi\frac{x}{\sqrt{\varepsilon}}\right) \\
& \times\exp\left(-\alpha\frac{x}{\sqrt{\varepsilon}}\right) + A_{00}^{(1)}\left(b_{01}^{(2)}\cos\phi\frac{\pi-x}{\sqrt{\varepsilon}} + b_{10}^{(2)}\sin\phi\frac{\pi-x}{\sqrt{\varepsilon}}\right)\exp\left(-\alpha\frac{\pi-x}{\sqrt{\varepsilon}}\right)\Bigg] \\
& + \varepsilon^3\Bigg[-B_{00}^{(3)}\frac{y^2}{2} + B_{02}^{(3)}\cos 2ny + A_{02}^{(2)}(\cos 2ny-1)\left(b_{01}^{(3)}\cos\phi\frac{x}{\sqrt{\varepsilon}} + b_{10}^{(3)}\sin\phi\frac{x}{\sqrt{\varepsilon}}\right) \\
& \times\exp\left(-\alpha\frac{x}{\sqrt{\varepsilon}}\right) + A_{02}^{(2)}(\cos 2ny-1)\left(b_{01}^{(3)}\cos\phi\frac{\pi-x}{\sqrt{\varepsilon}} + b_{10}^{(3)}\sin\phi\frac{\pi-x}{\sqrt{\varepsilon}}\right)\exp\left(-\alpha\frac{\pi-x}{\sqrt{\varepsilon}}\right)\Bigg] \\
& + \varepsilon^4\left[-B_{00}^{(4)}\frac{y^2}{2} - b_{00}^{(4)}\frac{x^2}{2} + B_{11}^{(4)}\sin mx\sin ny + B_{20}^{(4)}\cos 2mx + B_{02}^{(4)}\cos 2ny + B_{13}^{(4)}\sin mx\sin 3ny\right] + \mathrm{O}(\varepsilon^5)
\end{aligned}
\tag{33}
$$

$$
\begin{aligned}
\Psi_x = & \varepsilon^{3/2}\left[A_{00}^{(1)}c_{10}^{(3/2)}\sin\phi\frac{x}{\sqrt{\varepsilon}}\exp\left(-\alpha\frac{x}{\sqrt{\varepsilon}}\right) + A_{00}^{(1)}c_{10}^{(3/2)}\sin\phi\frac{\pi-x}{\sqrt{\varepsilon}}\exp\left(-\alpha\frac{\pi-x}{\sqrt{\varepsilon}}\right)\right] \\
& + \varepsilon^2[C_{11}^{(2)}\cos mx\sin ny] + \varepsilon^{(5/2)}\Bigg[A_{02}^{(2)}(\cos 2ny-1)c_{10}^{(5/2)}\sin\phi\frac{x}{\sqrt{\varepsilon}}\exp\left(-\alpha\frac{x}{\sqrt{\varepsilon}}\right) \\
& + A_{02}^{(2)}(\cos 2ny-1)c_{10}^{(5/2)}\sin\phi\frac{\pi-x}{\sqrt{\varepsilon}}\exp\left(-\alpha\frac{\pi-x}{\sqrt{\varepsilon}}\right)\Bigg] + \varepsilon^3[C_{11}^{(3)}\cos mx\sin ny] \\
& + \varepsilon^4[C_{11}^{(4)}\cos mx\sin ny + C_{20}^{(4)}\sin 2mx + C_{13}^{(4)}\cos mx\sin 3ny] + \mathrm{O}(\varepsilon^5)
\end{aligned}
\tag{34}
$$

$$
\begin{aligned}
\Psi_y = & \varepsilon^2[D_{11}^{(2)}\sin mx\cos ny] + \varepsilon^3\Bigg[D_{11}^{(3)}\sin mx\cos ny + D_{02}^{(3)}\sin 2ny - (A_{02}^{(2)}2n\beta\sin 2ny) \\
& \times\left(d_{01}^{(3)}\cos\phi\frac{x}{\sqrt{\varepsilon}} + d_{10}^{(3)}\sin\phi\frac{x}{\sqrt{\varepsilon}}\right)\exp\left(-\alpha\frac{x}{\sqrt{\varepsilon}}\right) - (A_{02}^{(2)}2n\beta\sin 2ny) \\
& \times\left(d_{01}^{(3)}\cos\phi\frac{\pi-x}{\sqrt{\varepsilon}} + d_{10}^{(3)}\sin\phi\frac{\pi-x}{\sqrt{\varepsilon}}\right)\exp\left(-\alpha\frac{\pi-x}{\sqrt{\varepsilon}}\right)\Bigg] \\
& + \varepsilon^4[D_{11}^{(4)}\sin mx\cos ny + D_{02}^{(4)}\sin 2ny + D_{13}^{(4)}\sin mx\cos 3ny] + \mathrm{O}(\varepsilon^5)
\end{aligned}
\tag{35}
$$

It is noted that in Eq. (33) for the case of movable straight edges $b_{00}^{(4)} = 0$. In order to satisfy boundary condition $w_1 = 0$ on $y = 0$, π straight edges, $A_{00}^{(1)}$ in Eq. (32) is expanded by Fourier sine series in the y-direction according to

$$\frac{4}{\pi} A_{00}^{(1)} \sum_{j=1,3,\ldots} \frac{1}{j} \sin jy \tag{36}$$

and remain a constant in the x-direction. Because of Eq. (32), the prebuckling deformation of the panel is nonlinear.

Note that Eqs. (32)–(35) are somewhat different from those of axially compressed cylindrical shells (Shen, 2002a). All of the coefficients in Eqs. (32)–(35) are related and can be expressed in terms of $A_{11}^{(2)}$, but for the sake of brevity the detailed expressions are not shown, whereas α and ϕ are given in detail in Appendix A.

Next, upon substitution of Eqs. (32)–(35) into the boundary condition (24c) and into Eqs. (25) and (26), the postbuckling equilibrium paths can be written as

$$\lambda_{\mathrm{p}} = \lambda_{\mathrm{p}}^{(0)} - \lambda_{\mathrm{p}}^{(2)} (A_{11}^{(2)} \varepsilon)^2 + \lambda_{\mathrm{p}}^{(4)} (A_{11}^{(2)} \varepsilon)^4 + \cdots \tag{37}$$

and

$$\delta_{\mathrm{p}} = \delta_{\mathrm{p}}^{(0)} - \delta_{\mathrm{p}}^{(\mathrm{T})} + \delta_{\mathrm{p}}^{(2)} (A_{11}^{(2)} \varepsilon)^2 + \delta_{\mathrm{p}}^{(4)} (A_{11}^{(2)} \varepsilon)^4 + \cdots \tag{38}$$

In Eqs. (37) and (38), $(A_{11}^{(2)} \varepsilon)$ is taken as the second perturbation parameter relating to the dimensionless maximum deflection. If the maximum deflection is assumed to be at the point $(x, y) = (\pi/2m, \pi/2n)$, from Eq. (32) one has

$$A_{11}^{(2)} \varepsilon = W_{\mathrm{m}} - \Theta_3 W_{\mathrm{m}}^2 + \cdots \tag{39a}$$

where W_{m} is the dimensionless form of maximum deflection of the panel that can be written as

$$W_{\mathrm{m}} = \frac{1}{C_3} \left[\frac{t}{[D_{11}^* D_{22}^* A_{11}^* A_{22}^*]^{1/4}} \frac{\overline{W}}{t} + \Theta_4 \right] \tag{39b}$$

All symbols used in Eqs. (37)–(39b) are also described in detail in Appendix A. It is noted that now $\lambda_{\mathrm{p}}^{(i)}$ and $\delta_{\mathrm{p}}^{(i)}$ $(i = 0, 2, 4, \ldots)$ are all functions of temperature and position.

Eqs. (37)–(39b) are employed to obtain numerical results for full nonlinear postbuckling load–shortening or load–deflection curves of FGM cylindrical panels subjected to axial compression in thermal environments. The initial buckling load of a perfect panel can readily be obtained numerically, by setting $\overline{W}^*/t = 0$, while taking $\overline{W}/t = 0$ (note that $W_{\mathrm{m}} \neq 0$). In this case, the minimum buckling load is determined by considering Eq. (37) for various values of the buckling mode (m, n), which determine the number of half-waves in the X- and Y-directions.

4. Numerical results and comments

Numerical results are presented in this section for FGM cylindrical panels with two constituent materials. Two sets of material mixture are considered. One is silicon nitride and stainless steel, referred to as Si_3N_4/SUS304, and the other is zirconium oxide and titanium alloy, referred to as ZrO_2/Ti–6Al–4V. However, the analysis is equally applicable to other types of FGMs. The material properties P, such as Young's modulus E and thermal expansion coefficient α, can be expressed as a function of temperature (see Touloukian, 1967) as

$$P = P_0 (P_{-1} T^{-1} + 1 + P_1 T + P_2 T^2 + P_3 T^3) \tag{40}$$

in which $T = T_0 + \Delta T$ and $T_0 = 300$ K (room temperature), P_0, P_{-1}, P_1, P_2 and P_3 are the coefficients of temperature T (K) and are unique to the constituent materials. Typical values for Young's modulus E (in Pa) and thermal expansion coefficient α (in K^{-1}) of these materials are listed in Table 1 (from Reddy and Chin, 1998). Poisson's ratio v is assumed to be a constant, and $v = 0.28$.

As part of the validation of the present method, the buckling loads for isotropic cylindrical panels subjected to axial compression are compared in Tables 2 and 3 with the numerical and analytical results based on the first order shear deformation theory obtained by Jaunky and Knight (1999), and the classical shell theory solutions of Turvey (1977). These two comparisons show that the results from the method presented agree well with the comparator solutions.

The buckling loads P_{cr} (in MN) for perfect Si_3N_4/SUS304 and ZrO_2/Ti–6Al–4V cylindrical panels with different values of volume fraction index N subjected to axial compression and under thermal environmental conditions are compared in Tables 4 and 5. In computation, the panel length-to-width ratio $a/b = 1.2$ and $b = 0.3$ m. It can be seen that, for the Si_3N_4/SUS304 cylindrical panel, a fully metallic panel ($N = 0$) has lowest buckling load and that the buckling load is increased as N increases. It can also be seen that the buckling load of the ZrO_2/Ti–6Al–4V cylindrical panel is lower than that of the Si_3N_4/SUS304 panel. Usually, the buckling loads are reduced with increases in temperature. In contrast, for ZrO_2/Ti–6Al–4V cylindrical panel ($a/R = 0.5$ and $b/t = 60$) the buckling load under thermal environmental condition $\Delta T = 200$ K is higher than that under thermal environmental condition $\Delta T = 0$ K, when $N > 3$. Therefore,

Table 1
Temperature-dependent coefficients for ceramics and metals, from Reddy and Chin (1998)

Materials		P_0	P_{-1}	P_1	P_2	P_3
Zirconia	E	244.27e+9	0	−1.371e−3	1.214e−6	−3.681e−10
	α	12.766e−6	0	−1.491e−3	1.006e−5	−6.778e−11
Silicon nitride	E	348.43e+9	0	−3.070e−4	2.160e−7	−8.946e−11
	α	5.8723e−6	0	9.095e−4	0	0
Ti–6Al–4V	E	122.56e+9	0	−4.586e−4	0	0
	α	7.5788e−6	0	6.638e−4	−3.147e−6	0
Stainless steel	E	201.04e+9	0	3.079e−4	−6.534e−7	0
	α	12.330e−6	0	8.086e−4	0	0

Table 2
Comparisons of buckling loads N_{cr} (in lbs/in) for isotropic cylindrical panels under axial compression ($E = 10 \times 10^6$ psi and $v = 0.3$)

a/b	a/R	b/t	Jaunky and Knight (1999)		Present HSDT
			FEM	Donnell-theory	
3.1831	10	78.5398	41945.4	53080.6	51419.68
3.1831	10	157.0796	12360.0	13834.1	13119.99
3.1831	10	314.1593	3358.8	3549.9	3228.12
1.5915	5	78.5398	50545.6	54817.2	53863.71
1.5915	5	157.0796	27020.0	28259.2	26239.99
0.7958	2.5	314.1593	14204.4	14378.4	13391.37

Table 3
Comparisons of buckling loads N_x/ER for isotropic cylindrical panels under axial compression ($v = 0.3$)

a/b	a/R	b/t	Turvey (1977) CLT	Present HSDT
4.0	1.0	25	0.73675e−4	0.71410e−4 (3,1)[a]
1.333	1.0	75	0.60523e−4	0.58737e−4 (2,2)

[a] The number in brackets indicate the buckling mode (m, n).

Table 4
Comparisons of buckling loads P_{cr} (in MN) for perfect Si_3N_4/SUS304 cylindrical panels subjected to axial compression and in thermal environments ($a/b = 1.2$, $b = 0.3$ m and $T_0 = 300$ K)

N	$a/R = 0.5$, $b/t = 30$		$a/R = 1.0$, $b/t = 30$		$a/R = 0.5$, $b/t = 60$	
	$\Delta T = 0$ K	$\Delta T = 200$ K	$\Delta T = 0$ K	$\Delta T = 200$ K	$\Delta T = 0$ K	$\Delta T = 200$ K
0	4.9565 (1,1)[a]	4.0541	10.2899 (3,1)	9.9258 (2,2)	1.2968 (1,3)	1.0906 (2,2)
0.2	5.4489	4.5268	11.3137	11.0764 (2,2)	1.4261	1.1919
0.5	5.8836	4.9672	12.2149	12.0141 (3,1)	1.5396	1.2778
1.0	6.2758	5.3811	13.0261	12.7691 (3,1)	1.6413	1.3579
2.0	6.6488	5.7845	13.7970	13.4870 (3,1)	1.7377	1.4429
3.0	6.8431	5.9947	14.1989	13.8614 (3,1)	1.7881	1.4933
5.0	7.0594	6.2257	14.6475	14.2797 (3,1)	1.8445	1.5561
8.0	7.2280	6.4023	14.9982	14.6071 (3,1)	1.8889	1.6098
10.0	7.2968	6.4734	15.1416	14.7412 (3,1)	1.9071	1.6328

[a] The number in brackets indicate the buckling mode (m, n).

Table 5
Comparisons of buckling loads P_{cr} (in MN) for perfect ZrO_2/Ti–6A1–4V cylindrical panels subjected to axial compression and in thermal environments ($a/b = 1.2$, $b = 0.3$ m and $T_0 = 300$ K)

N	$a/R = 0.5$, $b/t = 30$		$a/R = 1.0$, $b/t = 30$		$a/R = 0.5$, $b/t = 60$	
	$\Delta T = 0$ K	$\Delta T = 200$ K	$\Delta T = 0$ K	$\Delta T = 200$ K	$\Delta T = 0$ K	$\Delta T = 200$ K
0	2.5213 (1,1)[a]	2.1801	5.2343 (3,1)	4.6950 (3,1)	0.6596 (3,1)	0.5983 (2,2)
0.2	2.7891	2.2524	5.7912	5.1472 (3,1)	0.7300	0.5795
0.5	3.0253	2.2821	6.2808	5.5604 (2,2)	0.7916	0.5941
1.0	3.2386	2.2995	6.7219	5.6574 (2,2)	0.8469	0.6734
2.0	3.4420	2.3338	7.1422	5.7262 (2,2)	0.8995	0.8196
3.0	3.5481	2.3665	7.3618	5.7730 (2,2)	0.9270	0.9125
5.0	3.6663	2.4145	7.6070	5.8523 (2,2)	0.9579	1.0147
8.0	3.7584	2.4572	7.7985	5.9402 (2,2)	0.9821	1.0867
10.0	3.7960	2.4752	7.8768	5.9828 (2,2)	0.9920	1.1136

[a] The number in brackets indicate the buckling mode (m, n).

Si_3N_4/SUS304 cylindrical panels are considered in the parametric study only. Typical results are shown in Figs. 2–7. It is mentioned that in all figures $\overline{W}^*/t$ denotes the dimensionless maximum initial geometric imperfection of the panel.

Fig. 2 gives the postbuckling load–shortening and load–deflection curves for Si_3N_4/SUS304 cylindrical panels with volume fraction index $N = 2.0$ subjected to axial compression and under three sets of thermal environmental conditions, i.e. $\Delta T = 0$, 100 and 200 K. It can be seen that the well-known "snap-through" behavior of the panel occurs and the imperfection sensitivity can be predicted. It can also be found that the buckling loads and postbuckling strength are reduced with increases in temperature, but the postbuckling path becomes higher when the deflection is sufficiently large.

Fig. 3 gives the postbuckling load–shortening and load–deflection curves for Si_3N_4/SUS304 cylindrical panels with different values of volume fraction index N ($= 0.2$, 2.0 and 10.0) subjected to axial compression and under thermal environmental condition $\Delta T = 200$ K. It can be seen that the panel has lower buckling load and postbuckling path when it has lower volume fraction.

Fig. 4 shows the effect of width-to-thickness ratio b/t ($= 20$, 30 and 60) on the postbuckling behavior of Si_3N_4/SUS304 cylindrical panels with volume fraction index $N = 2.0$ subjected to axial compression and under thermal environmental condition $\Delta T = 200$ K. Then Fig. 5 shows the effect of length-to-width ratio a/b ($= 1.2$ and 2.5) on the postbuckling behavior of Si_3N_4/SUS304 cylindrical panels under the same

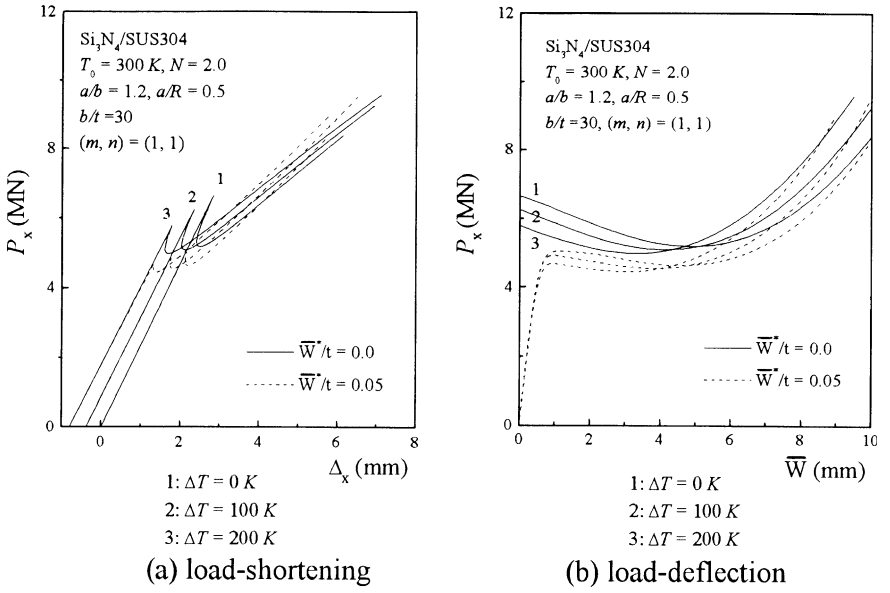

Fig. 2. Effect of temperature rise on the postbucking behavior of Si_3N_4/SUS304 cylindrical panels: (a) load–shortening and (b) load–deflection.

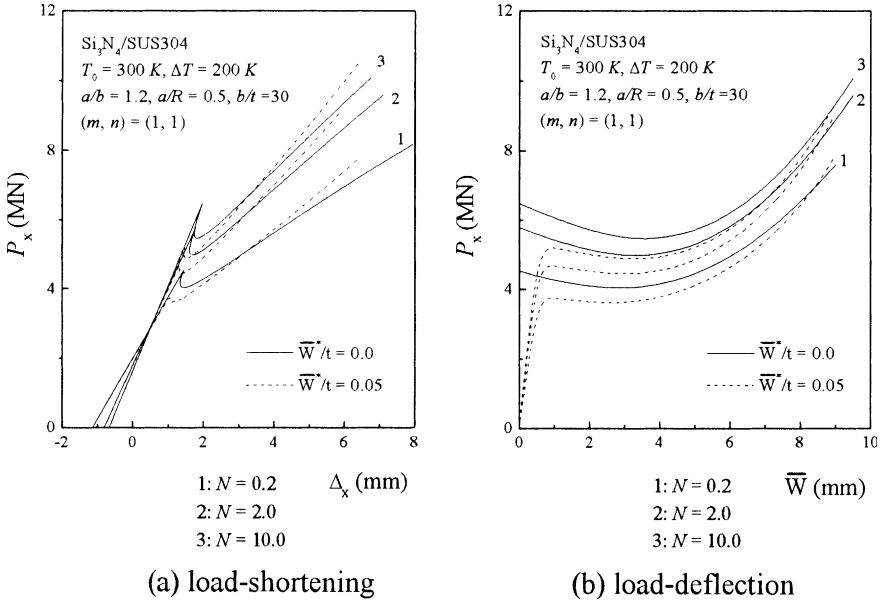

Fig. 3. Effect of volume fraction index N on the postbuckling behavior of Si_3N_4/SUS304 cylindrical panels: (a) load–shortening and (b) load–deflection.

condition. The results show that the buckling load is decreased as b/t increases from 20 to 60, or as a/b increases from 1.2 to 2.5 and the postbuckling equilibrium path becomes significantly lower. Changes of buckling mode can be seen for the panel with $b/t = 60$ or $a/b = 2.5$ and postbuckling equilibrium path becomes stable.

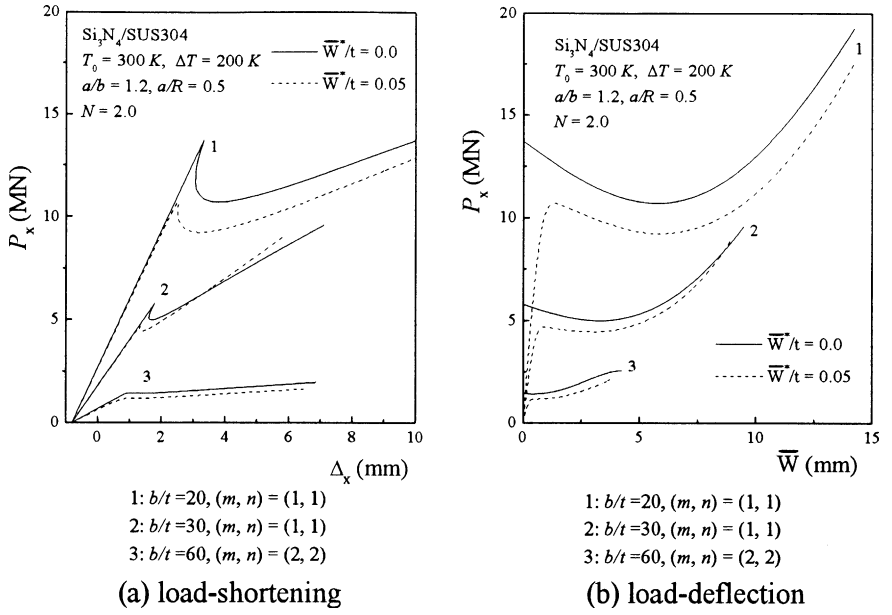

Fig. 4. Effect of width-to-thickness ratio on the postbuckling behavior of Si_3N_4/SUS304 cylindrical panels: (a) load–shortening and (b) load–deflection.

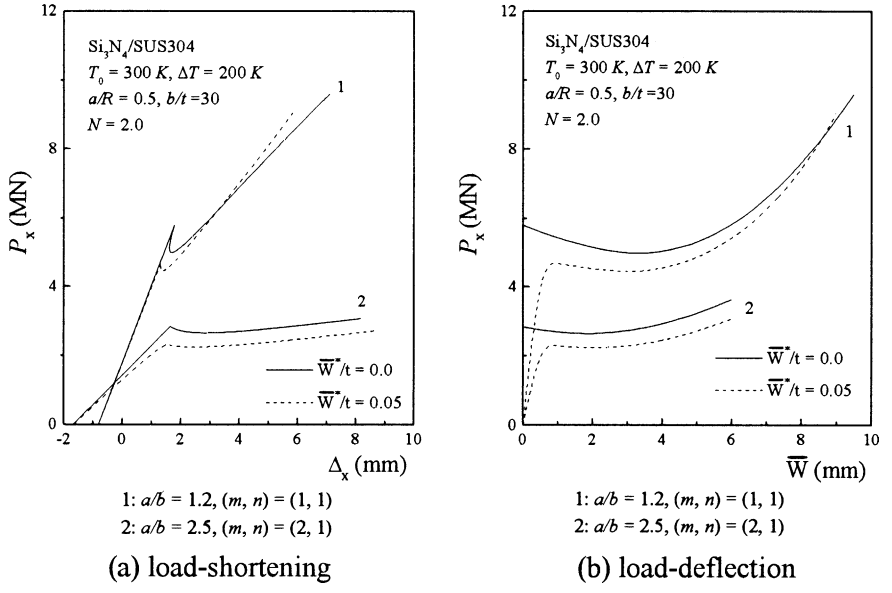

Fig. 5. Effect of length-to-width ratio on the postbuckling behavior of Si_3N_4/SUS304 cylindrical panels: (a) load–shortening and (b) load–deflection.

Fig. 6 shows the effect of length-to-radius ratio a/R ($=0.2$, 0.5 and 0.75) on the postbuckling behavior of Si_3N_4/SUS304 cylindrical panels with volume fraction index $N = 2.0$ subjected to axial compression and

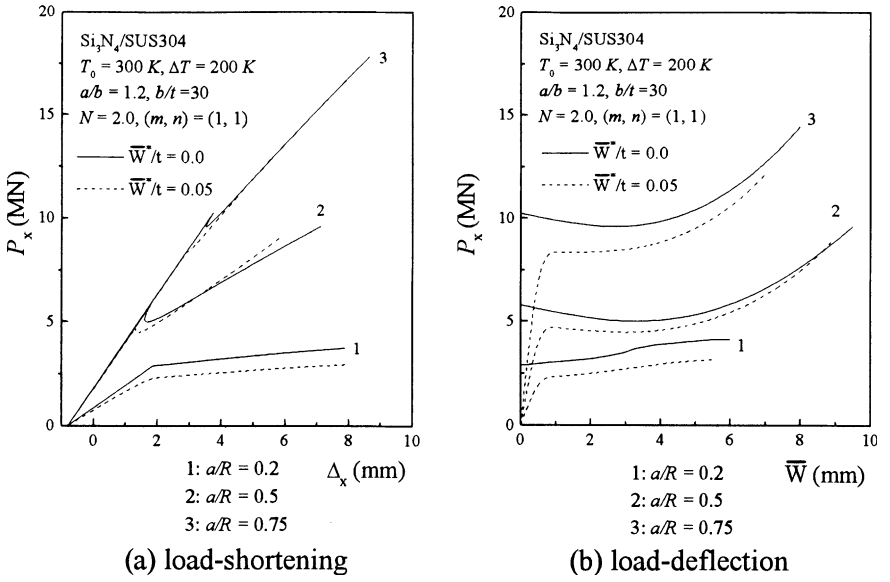

Fig. 6. Effect of length-to-radius ratio on the postbuckling behavior of Si_3N_4/SUS304 cylindrical panels: (a) load–shortening and (b) load–deflection.

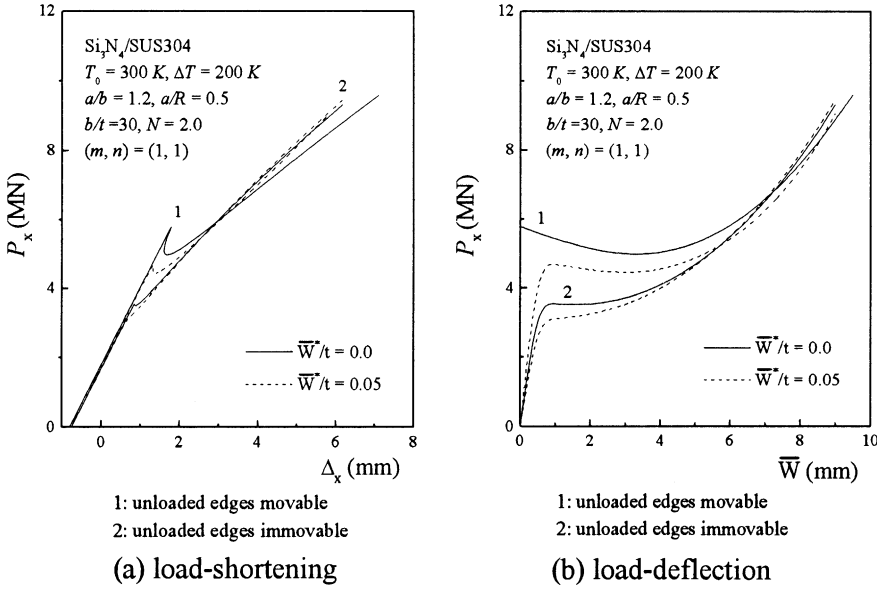

Fig. 7. Effect of in-plane boundary conditions on the postbuckling behavior of Si_3N_4/SUS304 cylindrical panels: (a) load–shortening and (b) load–deflection.

under thermal environmental condition $\Delta T = 200$ K. The results show that the panel with $a/R = 0.2$ has stable postbuckling equilibrium path due to its flatted configuration, while the panel with $a/R = 0.75$ has higher buckling load than others, and has considerable postbuckling strength.

Table 6
Imperfection sensitivity λ^* for imperfect Si_3N_4/SUS304 cylindrical panels ($a/b = 1.2$, $a/R = 0.5$, $b/t = 30$) with different values of volume fraction index N and under thermal environmental condition ($T_0 = 300$ K and $\Delta T = 0$ K)

$\overline{W}^*/t$	N		
	0.2	2.0	10.0
0	1.0	1.0	1.0
0.02	0.882	0.880	0.880
0.04	0.799	0.795	0.795
0.06	0.735	0.731	0.731
0.08	0.682	0.679	0.679
0.10	0.638	0.634	0.634
0.12	0.599	0.595	0.595
0.14	0.565	–	–

Fig. 7 compares postbuckling load–shortening and load–deflection curves for Si_3N_4/SUS304 cylindrical panels under two cases of the in-plane boundary conditions. It is noted that in the case of immovable edges the postbuckling path is no longer of the bifurcational type.

Postbuckling load–shortening and load–deflection curves for imperfect ($\overline{W}^*/t = 0.05$) as well as perfect ($\overline{W}^*/t = 0$) panels are plotted in each of Figs. 2–7. The imperfection sensitivity λ^* is calculated and compared in Table 6 for Si_3N_4/SUS304 cylindrical panels subjected to axial compression and under thermal environmental condition $\Delta T = 0$ K. Here, λ^* is the maximum value of σ_x for the imperfect panel, made dimensionless by dividing by the critical value of σ_x for the perfect panel as shown in Table 4. These results show that the volume fraction index N has a very small effect on the imperfection sensitivity of the panel.

5. Concluding remarks

In order to assess the effects of temperature rise and volume fraction index on the postbuckling behavior of FGM cylindrical panels subjected to axial compression, a fully nonlinear postbuckling analysis is presented based on Reddy's higher order shear deformation shell theory with a von Kármán–Donnell-type of kinematic nonlinearity. Material properties are assumed to be temperature dependent, and graded in the thickness direction according to a simple power law distribution in terms of the volume fractions of the constituents. The boundary layer theory of shell buckling has been extended to the case of FGM cylindrical panels subjected to compressive axial loads in thermal environments. A singular perturbation technique is employed to determine buckling loads and postbuckling equilibrium paths. Numerical results are for Si_3N_4/SUS304 and ZrO_2/Ti–6Al–4V cylindrical panels. In effect, the results provide information about postbuckling behaviors of FGM panels for different proportions of the ceramic and metal. The results reveal that the axially loaded FGM panel displays a complex form of postbuckling behavior which depends on the properties of the panel itself. They also confirm that the characteristics of postbuckling are significantly influenced by temperature rise, volume fraction distribution, panel geometric parameters as well as initial geometric imperfections.

Acknowledgements

This work is supported in part by the National Natural Science Foundation of China under Grant 59975058. The author is grateful for this financial support.

Appendix A

In Eq. (18)

$$A_x^{\mathrm{T}} = \frac{t}{1-\nu}\left\{(\alpha_{\mathrm{b}}-\alpha_{\mathrm{t}})(E_{\mathrm{b}}-E_{\mathrm{t}})\frac{1}{2N+1} + [\alpha_{\mathrm{t}}(E_{\mathrm{b}}-E_{\mathrm{t}}) + (\alpha_{\mathrm{b}}-\alpha_{\mathrm{t}})E_{\mathrm{t}}]\frac{1}{N+1} + \alpha_{\mathrm{t}}E_{\mathrm{t}}\right\} \tag{A.1}$$

and in Eqs. (37)–(39b)

$$\Theta_3 = \frac{1}{C_3}\left[\gamma_{14}\gamma_{24}\frac{m^4(1+\mu)}{8n^2\beta^2 g_{09}g_{06}}\varepsilon^{-1} - \gamma_{14}\gamma_{24}\frac{m^2 g_{11}}{16n^2\beta^2 g_{09}} + \frac{2\gamma_5}{\gamma_{24}}\lambda_{\mathrm{p}}^{(2)}\right]$$

$$\Theta_4 = \frac{1}{\gamma_{24}}[(\gamma_{\mathrm{T2}} - \gamma_5\gamma_{\mathrm{T1}})\Delta T] + \frac{2\gamma_5}{\gamma_{24}}\lambda_{\mathrm{p}}^{(0)}$$

$$\begin{aligned}\lambda_{\mathrm{p}}^{(0)} = \frac{1}{2}\Bigg\{ & \frac{\gamma_{24}m^2}{(1+\mu)g_{06}}\varepsilon^{-1} + \gamma_{24}\frac{g_{05}+(1+\mu)g_{07}}{(1+\mu)^2 g_{06}} \\ & + \frac{1}{\gamma_{14}(1+\mu)m^2}\left[g_{08} + \gamma_{14}\gamma_{24}\frac{g_{05}}{g_{06}}\frac{(1+\mu)g_{07} - \mu(2+\mu)g_{05}}{(1+\mu)^2}\right]\varepsilon \\ & - \frac{\mu}{(1+\mu^2)}\frac{g_{05}}{\gamma_{14}m^4}\left[1 + \frac{g_{05}}{(1+\mu)m^2}\varepsilon\right]\left[g_{08} + \gamma_{14}\gamma_{24}\frac{g_{05}}{g_{06}}\frac{g_{05}+(1+\mu)g_{07}}{(1+\mu)^2}(2+\mu)\right]\varepsilon^2\Bigg\}\end{aligned}$$

$$\begin{aligned}\lambda_{\mathrm{p}}^{(2)} = \frac{1}{8}\Bigg\{ & \gamma_{14}\gamma_{24}^2\frac{m^6(2+\mu)}{2g_{09}g_{06}^2}\varepsilon^{-1} + \gamma_{14}\gamma_{24}\frac{m^4}{2g_{09}g_{06}}\left[\frac{g_{05}}{g_{06}}\frac{1}{1+\mu} + \frac{g_{07}}{g_{06}}(1+\mu) + g_{12}(1+\mu) - \frac{1}{2}\frac{(2+\mu)}{(1+\mu)}g_{11}\right] - C_{22} \\ & + \gamma_{14}\gamma_{24}^2\frac{m^2 g_{11}}{2g_{09}}\left[\frac{g_{05}}{g_{06}}\frac{1}{1+\mu} - \frac{g_{07}}{g_{06}} - g_{12}\right]\varepsilon + \gamma_{14}\gamma_{24}^2\frac{m^2 g_{05}}{2g_{09}g_{06}}\left[\frac{2(1+\mu)^2 - (1+2\mu)}{2(1+\mu)^2}g_{14} + \frac{\mu}{1+\mu}\frac{g_{05}}{g_{06}}\right](2+\mu)\varepsilon \\ & + \gamma_{24}\frac{m^2n^4\beta^4}{g_{06}}\frac{(5+11\mu+4\mu^2)g_{06} + 8m^4(1+\mu)(2+\mu)g_{10}}{(1+\mu)g_{06} - 4m^4 g_{10}}\varepsilon\Bigg\}\end{aligned}$$

$$\lambda_{\mathrm{p}}^{(4)} = \frac{1}{128}\gamma_{14}^2\gamma_{24}^3\frac{m^{10}(1+\mu)}{g_{09}^2 g_{06}^3}\frac{(6+6\mu+\mu^2)g_{136} + (1+\mu)(6-\mu^2)g_{06}}{g_{136} - (1+\mu)g_{06}}\varepsilon^{-1} + C_{44}$$

$$\delta_{\mathrm{p}}^{(0)} = \frac{1}{\gamma_{24}}\left[\gamma_{24}^2 - \frac{2}{\pi}\frac{\gamma_5^2}{\gamma_{24}}\left(\alpha b_{01}^{(2)} - \phi b_{10}^{(2)}\right)\varepsilon^{1/2}\right]\lambda_{\mathrm{p}} + \left[\frac{\gamma_5^2}{2\pi\gamma_{24}^2}\frac{b_{11}}{\alpha}\varepsilon^{1/2}\right]\lambda_{\mathrm{p}}^2$$

$$\delta_{\mathrm{p}}^{(2)} = \frac{1}{16}\left[d_{22}(1+2\mu)\varepsilon - 2g_{05}\varepsilon^2 + \frac{g_{05}^2}{m^2}\varepsilon^3\right]$$

$$\delta_{\mathrm{p}}^{(4)} = \frac{1}{128}\left\{\frac{b_{11}}{32\pi\alpha}\gamma_{14}^2\gamma_{24}^2\frac{m^8(1+\mu)^2}{n^4\beta^4 g_{09}^2 g_{06}^2}\varepsilon^{-3/2} + d_{44} + m^2n^4\beta^4(1+\mu)^2\varepsilon^3\left[\frac{g_{06}(1+2\mu) + 8m^4(1+\mu)g_{10}}{g_{06}(1+\mu) - 4m^4 g_{10}}\right]^2\right\}$$

$$\delta_{\mathrm{p}}^{(\mathrm{T})} = \frac{1}{2\gamma_{24}}[(\gamma_{24}^2\gamma_{\mathrm{T1}} - \gamma_5\gamma_{\mathrm{T2}})\Delta T] \tag{A.2}$$

in the above equations (with other g_{ij} and g_{ijk} are defined as in Shen (2002c))

$$b_1 = \left[\frac{\gamma_{14}\gamma_{24}\gamma_{320}^2}{g_{16}}\right]^{1/2}, \quad c_1 = \gamma_{14}\gamma_{24}\gamma_{320}\frac{g_{15}}{2g_{16}}, \quad C_3 = 1 - \frac{g_{05}}{m^2}\varepsilon$$

$$\alpha = [(b_1 - c_1)/2]^{1/2}, \quad \phi = [(b_1 + c_1)/2]^{1/2}, \quad \mu = (a_{11}^* + A_{\mathrm{II}}^*)/A_{11}^{(2)}$$

$$a_{01}^{(1)} = 1, \quad a_{10}^{(1)} = g_{17}, \quad b_{01}^{(2)} = \gamma_{24}g_{19}, \quad b_{10}^{(2)} = \gamma_{24}g_{20}$$

$$b_{11} = \frac{1}{b_1}\left[\left(a_{10}^{(1)}\right)^2\phi^2 b_1 + a_{10}^{(1)}2\alpha\phi c_1 + \left(2\alpha^4 - \alpha^2\phi^2 + \phi^4\right)\right]$$

$$g_{17} = -\frac{(\gamma_{310} + \gamma_{14}\gamma_{24}\gamma_{220}\gamma_{240})c_1 + \gamma_{14}\gamma_{24}\gamma_{220}}{2\alpha\phi(\gamma_{310} + \gamma_{14}\gamma_{24}\gamma_{220}\gamma_{240})}$$

$$g_{19} = \frac{\gamma_{310}\gamma_{220} - \gamma_{320}\gamma_{240}}{\gamma_{320} + \gamma_{14}\gamma_{24}\gamma_{220}^2} - \frac{2c_1(\gamma_{310} + \gamma_{14}\gamma_{24}\gamma_{220}\gamma_{240}) + \gamma_{14}\gamma_{24}\gamma_{220}\gamma_{320}}{(\gamma_{320} + \gamma_{14}\gamma_{24}\gamma_{220}^2)(\gamma_{310} + \gamma_{14}\gamma_{24}\gamma_{220}\gamma_{240})b_1^2}$$

$$g_{20} = -\frac{1}{2\alpha\phi(\gamma_{310} + \gamma_{14}\gamma_{24}\gamma_{220}\gamma_{240})(\gamma_{320} + \gamma_{14}\gamma_{24}\gamma_{220}^2)}\left[\gamma_{310}\left(\gamma_{320} + \gamma_{14}\gamma_{24}\gamma_{220}^2\right) - 2(\gamma_{310} + \gamma_{14}\gamma_{24}\gamma_{220}\gamma_{240})\frac{c_1^2}{b_1^2}\right.$$
$$\left. - \gamma_{14}\gamma_{24}\gamma_{220}\gamma_{320}\frac{c_1}{b_1^2} + (\gamma_{310} + \gamma_{14}\gamma_{24}\gamma_{220}\gamma_{240})(\gamma_{310}\gamma_{220} - \gamma_{320}\gamma_{240})c_1\right] \tag{A.3}$$

for the case of immovable straight edges

$$A_{\mathrm{II}}^* = \frac{2\gamma_{14}\gamma_{24}n^2\beta^2}{\pi^2 mng_{08}}(1+2\mu)\left(A_{11}^{(2)}\right)^2, \quad C_{22} = \frac{1}{4}\gamma_{24}g_{13}\frac{\left(m^4 + 2\gamma_{24}^2n^4\beta^4\right)}{m^2}(1+2\mu)\varepsilon,$$
$$C_{44} = \frac{1}{128}\frac{\gamma_{14}^2\gamma_{24}^2m^6(1+\mu)^2}{4g_{09}^2g_{06}^2}\varepsilon^{-1}, \quad d_{22} = m^2 + \gamma_5n^2\beta^2, \quad d_{44} = \frac{\gamma_5\gamma_{14}^2\gamma_{24}}{4}\frac{m^8(1+\mu)^2}{n^2\beta^2g_{09}^2g_{06}^2}\varepsilon^{-1} \tag{A.4}$$

and for the case of movable straight edges

$$A_{\mathrm{II}}^* = 0, \quad C_{22} = \tfrac{1}{4}\gamma_{24}m^2g_{13}(1+2\mu)\varepsilon, \quad C_{44} = 0, \quad d_{22} = m^2, d_{44} = 0 \tag{A.5}$$

References

Chang, M.Y., Librescu, L., 1995. Postbuckling of shear deformable flat and curved panels under combined loading conditions. International Journal of Mechanical Sciences 37, 121–143.

Chia, C.Y., 1987. Nonlinear vibration and postbuckling of unsymmetrically laminated imperfect shallow cylindrical panels with mixed boundary conditions resting on elastic foundation. International Journal of Engineering Science 25, 427–441.

Huang, N.N., Taucher, T.R., 1991. Large deflections of laminated cylindrical and doubly-curved panels under thermal loading. Computers and Structures 41, 303–312.

Jaunky, N., Knight, N.F., 1999. An assessment of shell theories for buckling of circular cylindrical laminated composite panels loaded in axial compression. International Journal of Solids and Structures 36, 3799–3820.

Koizumi, M., 1993. The concept of FGM. Ceramic Transactions, Functionally Gradient Materials 34, 3–10.

Kweon, J.H., Hong, C.S., 1994. An improved arc-length method for postbuckling analysis of composite cylindrical panels. Computers and Structures 53, 541–549.

Kweon, J.H., Hong, C.S., Lee, I.C., 1995. Postbuckling compressive strength of graphite/epoxy laminated cylindrical panels loaded in compression. American Institute of Aeronautics and Astronautics Journal 33, 217–222.

Librescu, L., Nemeth, M.P., Starnes, J.H., Lin, W., 2000. Nonlinear response of flat and curved panels subjected to thermomechanical loads. Journal of Thermal Stresses 23, 549–582.

Loy, C.T., Lam, K.Y., Reddy, J.N., 1999. Vibration of functionally graded cylindrical shells. International Journal of Mechanical Sciences 41, 309–324.

Ng, T.Y., Lam, K.Y., Liew, K.M., Reddy, J.N., 2001. Dynamic stability analysis of functionally graded cylindrical shells under periodic axial loading. International Journal of Solids and Structures 38, 1295–1309.

Pradhan, S.C., Loy, C.T., Lam, K.Y., Reddy, J.N., 2000. Vibration characteristics of functionally graded cylindrical shells under various boundary conditions. Applied Acoustics 61, 111–129.

Reddy, J.N., Liu, C.F., 1985. A higher-order shear deformation theory of laminated elastic shells. International Journal of Engineering Science 23, 319–330.

Reddy, J.N., Chin, C.D., 1998. Thermoelastical analysis of functionally graded cylinders and plates. Journal of Thermal Stresses 21, 593–626.

Shen, H.-S., 1997a. Post-buckling analysis of imperfect stiffened laminated cylindrical shells under combined external pressure and axial compression. Computers and Structures 63, 335–348.

Shen, H.-S., 1997b. Thermal postbuckling analysis of imperfect stiffened laminated cylindrical shells. International Journal of Non-Linear Mechanics 32, 259–275.

Shen, H.-S., 1997c. Thermomechanical postbuckling analysis of stiffened laminated cylindrical shell. Journal of Engineering Mechanics ASCE 123, 433–443.

Shen, H.-S., 1998. Postbuckling analysis of imperfect stiffened laminated cylindrical shells under combined external pressure and thermal loading. International Journal of Mechanical Sciences 40, 339–355.

Shen, H.-S., 2001a. The effects of hygrothermal conditions on the postbuckling of shear deformable laminated cylindrical shells. International Journal of Solids and Structures 38, 6357–6380.

Shen, H.-S., 2001b. Postbuckling of shear deformable cross-ply laminated cylindrical shells under combined external pressure and axial compression. International Journal of Mechanical Sciences 43, 2493–2523.

Shen, H.-S., 2002a. Postbuckling of shear deformable laminated cylindrical shells. Journal of Engineering Mechanics ASCE 128, 296–307.

Shen, H.-S., 2002b. Postbuckling analysis of axially loaded functionally graded cylindrical shells in thermal environments. Composites Science and Technology 62, 977–987.

Shen, H.-S., 2002c. Nonlinear bending response of functionally graded plates subjected to transverse loads and in thermal environments. International Journal of Mechanical Sciences 44, 561–584.

Shen, H.-S., Chen, T.-Y., 1988. A boundary layer theory for the buckling of thin cylindrical shells under external pressure. Applied Mathematics and Mechanics 9, 557–571.

Shen, H.-S., Chen, T.-Y., 1990. A boundary layer theory for the buckling of thin cylindrical shells under axial compression. In: Chien, W.Z., Fu, Z.Z. (Eds.), Advances of Applied Mathematics and Mechanics in China, vol. 2. International Academic Publishers, Beijing, China, pp. 155–172.

Touloukian, Y.S., 1967. Thermophysical Properties of High Temperature Solid Materials. McMillan, New York.

Turvey, G.J., 1977. Buckling of simply supported cross-ply cylindrical panels on elastic foundations. Aeronautical Journal 81, 88–91.

Vol'mir, A.A., 1967. Flexible Plates and Shells. AFFDL-TR-66-216.

Zhang, Y., Matthews, F.L., 1985. Large deflection behavior of simply supported laminated panels under in-plane loading. Journal of Applied Mechanics ASME 52, 553–558.